

Transient phases and dynamical transitions in the post-quench evolution of the generalized Bose-Anderson model

Dmitry V. Chichinadze,^{1,2,*} Pedro Ribeiro,^{3,2} Yulia E. Shchadilova,^{4,2} and Alexey N. Rubtsov^{2,1}

¹*Department of Physics, Lomonosov Moscow State University, Leninskie gory 1, 119991 Moscow, Russia*

²*Russian Quantum Center, Novaya 100, 143025 Skolkovo, Moscow Region, Russia*

³*CeFEMA, Instituto Superior Técnico, Universidade de Lisboa Av. Rovisco Pais, 1049-001 Lisboa, Portugal*

⁴*Department of Physics, Harvard University, Cambridge, Massachusetts 02138, USA*

(Received 19 April 2016; revised manuscript received 14 July 2016; published 1 August 2016)

The exact description of the time evolution of open correlated quantum systems remains one of the major challenges of condensed matter theory, especially for asymptotic long times where most numerical methods fail. Here, the post-quench dynamics of the N -component Bose-Anderson impurity model is studied in the $N \rightarrow \infty$ limit. The equilibrium phase diagram is similar to that of the Bose-Hubbard model in that it contains local versions of Mott and Bose phases. Using a numerically exact procedure, we are able to study the real-time evolution including asymptotic long-time regimes. The formation of long-lived transient phases is observed for quench paths crossing foreign phases. For quenches inside the local Bose condensed phase, a dynamical phase transition is reported that separates the evolution towards a new equilibrium state and a regime characterized at large times by a persistent phase rotation of the order parameter. We explain how such nondecaying modes can exist in the presence of a dissipative bath. We discuss the extension of our results to the experimentally relevant finite- N case and their implication for the existence of nondecaying modes in generic quantum systems in the presence of a bath.

DOI: [10.1103/PhysRevB.94.054301](https://doi.org/10.1103/PhysRevB.94.054301)

I. INTRODUCTION

The study of out-of-equilibrium processes in correlated quantum systems is a rapidly growing field. Progress has been driven by experimental advances in solid state and ultracold atomic setups that made possible the preparation, manipulation, and probing of quantum many-body states in real time. On the theory side, the study of correlated systems far from equilibrium gives rise to a set of new concepts, including transient order-enhanced phases [1], prethermalized transient states [2–5], prethermalization at a quantum critical point [6], and ordered current-carrying steady states [7–9].

A particularly interesting phenomenon arising in autonomous quantum systems, but yet poorly understood for open ones [10–12], is the occurrence of dynamical phase transitions. A dynamical transition is a singular point in the space of the couplings that parametrizes the quenching protocol where an infinitesimal difference in parameters yields a qualitative difference for the asymptotic long-time state. First reported for quenches of integrable Bardeen-Cooper-Schrieffer model [13–16], dynamical transitions were observed on a number of autonomous systems and studied using different methods [17–22]. For open systems, the fundamental question of whether a dynamical transition can arise in the presence of an environment remains unanswered. The coupling to a thermostat induces relaxation in the dynamics and subsequent decay to the equilibrium state. This process is expected to destroy the qualitative difference between the phases separated by the transition, thus broadening it to a crossover.

In this paper, we show that impurity models may be excited to a set of states that are completely decoupled

from the environment, therefore avoiding relaxation and ensuring the existence of a dynamical transition. Figure 1 illustrates the long-time post-quench evolution of the order

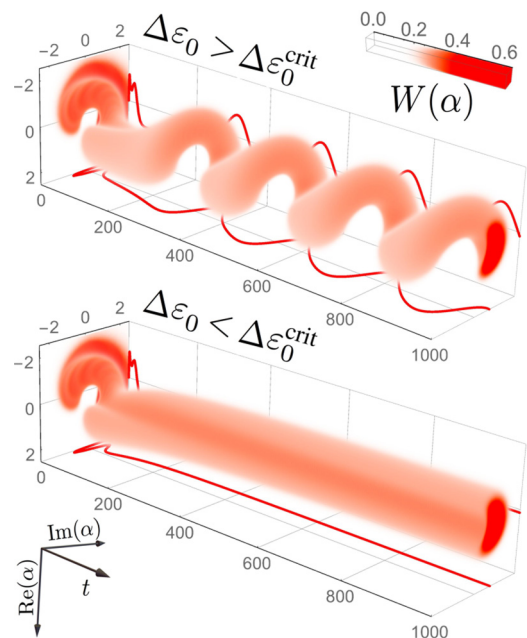


FIG. 1. Post-quench time dependence of the Husimi function of the generalized Bose-Anderson model: $W = |\langle \alpha | \Psi(t) \rangle|^2 / \langle \alpha | \alpha \rangle$; $|\alpha\rangle = e^{\alpha a^\dagger - \alpha^* a} |0\rangle$. The system was quenched between two points within the local Bose-Einstein condensed phase (D series in the Fig. 3). Dependent on the value of the quench, the system evolves either to the new equilibrium state (lower panel) or to the stable excited state exhibiting a persistent phase rotation of the order parameter (upper panel).

*Correspondence should be addressed: dchichinadze@gmail.com

parameter. It shows the Husimi function of a localized interacting bosonic mode coupled to a reservoir. The lower panel depicts the expected relaxation to the equilibrium state. One can observe that in the relaxational regime the phase of the order parameter stops rotating for long times. The upper panel shows how the broken-symmetry phase develops when the magnitude of the quench is large. It is worth observing that in the latter case the phase of the order parameter remains rotating for long times. In our work, we show that the system indeed exhibits frictionless rotation of the order parameter and that a decoupling from the thermostat is realized for a particular direction of the rotation (counterclockwise). We will demonstrate that the post-quench evolution yields one of these two situations: either the equilibrium state or the state with persistent phase oscillations, and that these two regimes are separated by a dynamical transition.

We address these questions by considering a particular example, the Bose-Anderson single-impurity model (B-SIAM) [23–25], describing a correlated impurity coupled to an infinite number of noninteracting bosonic lattice modes. Albeit their apparent simplicity, the physics of impurity models is extremely rich. Perhaps the most paradigmatic example of an impurity system is the celebrated Kondo model [26] that has permitted to explain the resistance minimum of certain metallic compounds. Some impurity systems undergo so-called impurity phase transitions [27–29] where local response and correlation functions become singular and can be characterized by a set of critical exponents. At these zero-temperature transitions, only a nonextensive term in the free energy becomes singular. Examples of widely studied quantum critical models are the pseudogap Kondo [30], the spin-boson [31], or the two-impurity Kondo model [30].

Quenched dynamics in impurity models has been considered in the context of electronic transport on quantum dots [32–36] and impurities in the quantum gases [37–39]. For systems with impurity phase transitions, quenches have been studied for the pseudogap Kondo model [40,41] and for the spin-boson problem [42,43]. However, whether dynamical transitions are to be seen in impurity models is an open question. If present, they have to be of a different nature of their extended counterparts. In the same way, the existence of transient long-lived phases is a possibility not yet explored for impurity systems.

The B-SIAM, addressed in this work, is of particular interest as it possesses a rich phase diagram with a set of impurity phase transition lines. Recent progress in the manipulation of ultracold atomic gases rendered the controlled realization of this model at experimental reach using optical lattices with single-site resolution [44]. This technique allows to manipulate localized potentials in real time. Creating local correlated defects allows for the possibility of studying bosonic impuritylike systems, analogous to magnetic impurities or quantum dots in solid-state devices, with the crucial advantage of being able to probe the dynamics in real time.

Equilibrium studies of the B-SIAM, by numerical renormalization group [23,24] and exact diagonalization [25], revealed a zero-temperature phase diagram containing high-symmetry phases, where number of excitations in the local node is an integer, and a broken-symmetry phase. As these

phases are local counterparts of the Mott and superfluid phases, observed for example in the Bose-Hubbard model on a lattice [45,46], they are dubbed local Mott insulator (IMI) and local Bose-Einstein condensate (IBEC) in the following. The local spectral function was shown to behave in a power-law fashion near zero frequency, with a negative exponent in the IBEC and a positive one in the IMI [24] that depend on the density of states of the bosonic environment. To our knowledge, there were no previous attempts to study this model away from equilibrium.

A number of works consider interaction quenches in extended systems featuring Mott and superfluid phases such as the Bose-Hubbard lattice model [3,47–54]. Here, as the energy injected into the system is extensive, the relaxation to the new ground state is forbidden by energy conservation. Instead, the system was found to approach either a thermalized or a nonthermalized state depending on the quench magnitude [3], with a dynamical transition separating the two regimes. Here, again, the presence of a thermostat is expected to dramatically change this picture since it induces relaxation of both thermal and nonthermal states eventually transforming the dynamical transition to a crossover. Numerically resolving between a dynamical transition and crossover regime in quantum many-body systems might be a challenging task. This problem is particularly difficult as it requires numerically exact methods to achieve long times. For example, real-time quantum Monte Carlo solvers suffer from the sign (phase) problem [34], whereas density matrix renormalization group (DMRG) [55] and exact diagonalization [56] are limited by the dimension of the basis of wave functions used. Moreover, approximate schemes approaches such as noncrossing approximation impurity solver [54] also suffer from memory issues raising at the long-time scale.

In this paper, we address the existence of dynamical transitions by studying the dynamics after a quench of the Bose-Anderson single-impurity model generalized to N components. The number of components N controls lattice quantum fluctuations and ensues an exact solution in the $N \rightarrow \infty$ limit [57], therefore allowing for the study of the full nonequilibrium dynamics of the system with a small numerical effort. We observe a variety of after-quench dynamical patterns, including relaxation to the equilibrium state, intermediate states qualitatively different from the initial and final ones, the formation of so-called transient phases, and stable recurrent states. We provide numerical evidence and physical argumentation that these recurrent states are indeed completely decoupled from the lattice thermostat. Hence, a dynamical transition is found, that separates the evolution from asymptotically reaching the equilibrium or leading to stable recurrent states. Finally, we argue that most of these effects hold for finite values of N , rendering our findings of immediate experimental relevance.

The structure of the paper is as follows. We present the model and methods in Sec. II. In Sec. III, we expose our results, including the equilibrium phase diagram and the qualitative different quench types. We present an integrated discussion of the results and develop some analytic arguments in Sec. IV. We conclude in Sec. V. The Appendix is devoted to the formal proof of the exactness of our method for large N .

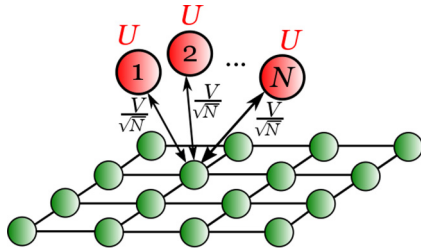


FIG. 2. Sketch of the generalized Bose-Anderson model. N impurities are coupled to the lattice at the same point with the same coupling constant $\frac{V}{\sqrt{N}}$. The onsite interaction $\frac{U}{2}n(n-1)$ occurs only at the impurities.

II. MODEL AND METHOD

We consider an impurity with N components, connected to a bosonic lattice on a single site, as shown in Fig. 2. This model is described by the generalized multicomponent Bose-Anderson Hamiltonian:

$$H = \sum_j H_{\text{SI}}[a_j^\dagger a_j] - \sum_{j,k} \frac{V_k}{\sqrt{N}} (a_j^\dagger b_k + \text{H.c.}) + \sum_k \epsilon_k b_k^\dagger b_k, \quad (1)$$

where

$$H_{\text{SI}}[a^\dagger a] = \epsilon_0 a^\dagger a + \frac{U}{2} a^\dagger a^\dagger a a \quad (2)$$

is the Hamiltonian of a single component. The operator a_j^\dagger , with $j = 1, \dots, N$, creates a j -component boson at the impurity site, ϵ_0 is the depth of the impurity onsite potential, and U is the local interaction strength. The operator b_k^\dagger creates a boson in mode k , ϵ_k is the lattice dispersion, and V_k/\sqrt{N} is the hopping amplitude between the bath and the impurity. In this paper, we define the energy scale by the condition $\hbar = 1$. We assume that ϵ_k has a single minimum near $\epsilon_{k=0} = 0$. The mode with $k = 0$ is excluded from the calculations to get rid of the effects, related to bulk BEC [25]. In the following, we consider that the dispersion relation of the bosonic bath is taken to be that of a three-dimensional cubic lattice $\epsilon_k = 2h(3 - \cos k_x - \cos k_y - \cos k_z)$, where h is the hopping matrix element. We set $h = 1$, $U = 1$. As the impurity is coupled to a single lattice site $V_k = V$ is independent of k . The considered quench parameters are either the onsite energy $\epsilon_0(t) = \theta(-t)\epsilon_0(0) + \theta(t)\epsilon_0$ or the impurity-bath coupling $V(t) = \theta(-t)V(0) + \theta(t)V$. In the limit $N = 1$, this model becomes the single-impurity Bose-Anderson model [23–25]. The rescaling in the hopping amplitudes is introduced in order to obtain a well-defined large- N limit.

In the following, we give a derivation of the equations ruling the dynamics of the model in the large- N limit, assuming an equilibrium zero-temperature initial state. An alternative derivation, using nonequilibrium Green's functions, valid also at finite T is given in the Appendix. For the $T = 0$ case, we consider the separable ansatz for the wave function

$$|\Psi\rangle = |\Psi_{\text{bath}}\rangle \otimes |\Psi_{\text{imp}}\rangle, \quad (3)$$

derive the equations of motion for both $|\Psi_{\text{bath}}\rangle$ and $|\Psi_{\text{imp}}\rangle$, and show this treatment becomes exact for $N \rightarrow \infty$. For finite N , this ansatz can be seen as mean-field-like approximation.

With the factorized wave function (3), two effective Hamiltonians $H_{\text{imp}}^{\text{eff}} \equiv \langle \Psi_{\text{bath}} | H | \Psi_{\text{bath}} \rangle$ and $H_{\text{bath}}^{\text{eff}} \equiv \langle \Psi_{\text{imp}} | H | \Psi_{\text{imp}} \rangle$ can be defined for the impurity and the bath, respectively. The effective dynamics is given by the two Schrödinger equations

$$i \partial_t |\Psi_{\text{imp}}\rangle = H_{\text{imp}}^{\text{eff}} |\Psi_{\text{imp}}\rangle,$$

$$i \partial_t |\Psi_{\text{bath}}\rangle = H_{\text{bath}}^{\text{eff}} |\Psi_{\text{bath}}\rangle$$

coupled through the dependence of the effective Hamiltonians on the instantaneous mean values of the bath or impurity observables.

The impurity effective Hamiltonian $H_{\text{imp}}^{\text{eff}} = \sum_j H_{\text{SI}}^{\text{eff}}[a_j^\dagger a_j]$, factorizes into a sum over independent components

$$H_{\text{SI}}^{\text{eff}}[a^\dagger a] = \epsilon_0 a^\dagger a + \frac{U}{2} a^\dagger a^\dagger a a - \lambda a^\dagger - \lambda^* a, \quad (4)$$

where we have introduced the parameter

$$\lambda = \sum_k \frac{V_k}{\sqrt{N}} \beta_k, \quad (5)$$

with $\beta_k = \langle b_k \rangle$.

The bath effective Hamiltonian is given by

$$H_{\text{bath}}^{\text{eff}} = \sum_k \epsilon_k b_k^\dagger b_k - \sum_{k,j} \frac{V_k}{\sqrt{N}} (b_k^\dagger \langle a_j \rangle + \langle a_j^\dagger \rangle b_k). \quad (6)$$

Note that, since all the components interact equally with the bath and we assume a component-symmetric initial condition, all $\langle a_j \rangle$ are the same and thus $\sum_j \langle a_j \rangle = N \langle a \rangle$. Similarly, other componentwise averages are independent of the component index: $\langle n_j \rangle \equiv \langle a_j^\dagger a_j \rangle = \langle n \rangle$, $\langle n_j^2 \rangle - \langle n_j \rangle^2 = \Delta^2 n$, etc. Thus, further in the text we will appeal to the averages per component $\langle a \rangle, \langle n \rangle$.

The equation for the mean value of b_k then reads as

$$-i \frac{d\beta_k}{dt} = \langle [H_{\text{bath}}^{\text{eff}}, b_k] \rangle = -\epsilon_k \beta_k + V_k \sqrt{N} \langle a \rangle, \quad (7)$$

which in its integral form yields

$$\beta_k(t) = \beta_k(0) e^{-i\epsilon_k t} + i V_k \sqrt{N} \int_0^t \langle a(t') \rangle e^{-i\epsilon_k(t-t')} dt'. \quad (8)$$

With this expression, the value of λ in Eq. (5) becomes

$$\lambda(t) = \sum_k V_k^2 \frac{e^{-i\epsilon_k t}}{\epsilon_k} \langle a(0) \rangle + i \sum_k V_k^2 \int_0^t \langle a(t') \rangle e^{-i\epsilon_k(t-t')} dt'. \quad (9)$$

Equation (4) together with (9) form a closed set of equations describing the effective dynamics of the multicomponent Bose-Anderson Hamiltonian after a quench. The initial condition is assumed to be the equilibrium solution before the quench is performed. $\lambda(0)$ is computed solving the self-consistent condition obtained from Eqs. (4) and (9) at $t = 0$.

Note that the considered ansatz wave function amounts, for this model, to consider the bath in the coherent state:

$$|\Psi_{\text{bath}}\rangle = \prod_k e^{\beta_k b_k^\dagger - \beta_k^* b_k} |0\rangle. \quad (10)$$

Let us now argue on physical grounds why this ansatz becomes exact in the limit of infinite N . According to Eqs. (7) and (10), the displacement of lattice modes scales as $\langle b_k \rangle \propto$

\sqrt{N} . For large N , this means that the lattice oscillators are in the classical regime and thus become c numbers in the limit of infinite N . Each lattice mode is thus described by a single value $\langle b_k \rangle$, which obeys the classical equation of motion (7). The evolution of the impurity can be found assuming a factorized form for the wave function $|\Psi_{\text{imp}}\rangle = |\Psi_{\text{SI}}\rangle_1 \otimes \dots \otimes |\Psi_{\text{SI}}\rangle_N$ that is exact once the bath modes are c numbers. The wave function $|\Psi_{\text{SI}}\rangle$ obeys the Schrödinger equation with the single-component Hamiltonian (4). Equation (4) describes a single-bosonic mode, it is thus amenable to be treated numerically. The formal proof that the separable ansatz is exact in the limit $N \rightarrow \infty$ is given the Appendix.

III. RESULTS

In this section, first we present the equilibrium phase diagram of the system and describe the distinct phases. In the following subsection, we discuss the numerical results for the evolution of the system after quenches of the system parameter. The initial state is always taken to be the ground state of the starting phase. In all further calculations, we consider time t in units of inverse hopping energy \hbar^{-1} .

A. Equilibrium

The equilibrium phase diagram of the generalized Bose-Anderson model is shown in the Fig. 3. The results were obtained solving the self-consistent condition of Eqs. (4) and (9) at equilibrium [that is, assuming all time derivatives in Eq. (7) are equal to zero]. The phase diagram encompasses two phases: a set of IMI lobes with a vanishing order parameter $\langle a \rangle$, and a IBEC phase where $\langle a \rangle \neq 0$. In the IBEC, a finite value of $\langle a \rangle$ implies nonvanishing fluctuations of the number of particles at impurity site $\Delta^2 n > 0$. Moreover, the number of particles $\langle n \rangle$ is not restricted to be an integer. The number of particles on the lattice is given by the expression $\sum_k \langle b_k^\dagger b_k \rangle = N \sum_k V_k^2 \frac{|a|^2}{\epsilon_k^2}$. For a d -dimensional lattice with $d < 4$ at $V_k = V$, the sum diverges in the thermodynamic limit whenever $\langle a \rangle \neq 0$, thus indicating the formation of a BEC.

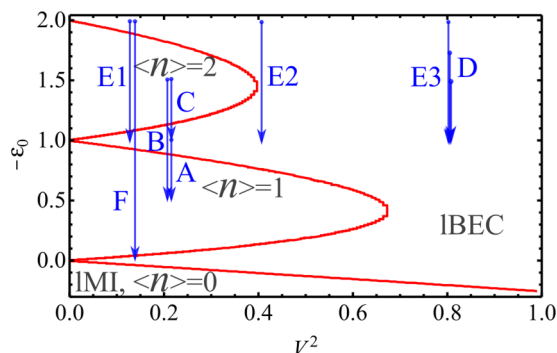


FIG. 3. Equilibrium phase diagram of generalized Bose-Anderson model at $U = 1, h = 1$. Different lobes correspond to a local Mott insulator phase with a different number of bosons per mode. The local Bose-Einstein condensate is characterized by nonvanishing values of the order parameter. The blue arrows depict the set of initial and final conditions characterizing the quench protocols considered in the paper.

Note that the bulk of the lattice lacks the BEC mode $k = 0$ since for convenience it is not considered here, therefore, $\sum_k \langle b_k^\dagger b_k \rangle \rightarrow \infty$ signals the formation of the BEC cloud in the vicinity of the impurity. The IMI phase is characterized by an integer number of bosons at the impurity site, i.e., $\langle n \rangle \in \mathbb{N}_0^+$ and $\Delta^2 n = 0$. Since $\langle a \rangle = 0$, lattice modes are not populated in this phase.

The phase diagram is qualitatively similar to the single-impurity Bose-Anderson model as obtained by numerical renormalization group approach [23,24] and by the exact diagonalization method [25]. The nomenclature of the phases is reminiscent of the Bose-Hubbard model [45,46] equilibrium phase diagrams.

In the following subsections, we consider the dynamics of the system after the instantaneous change of the chemical potential on the impurity site. Figure 3 depicts the set of different quenches under consideration. Quench protocols are characterized by the initial and final conditions. For each quench, we study the time evolution of the local order parameter $\langle a \rangle$ and of the number of particles per mode at the impurity site.

B. Quenches to the IMI phase

IBEC-IMI quench. First of all let, us consider the evolution of the system in the IBEC phase after the instantaneous change of the local energy on the impurity site. We choose the final value of the local chemical potential such as the final state corresponds to the IMI phase at the equilibrium phase diagram. In Fig. 4, the evolution of the local order parameter is shown after the quench, which is schematically depicted with arrow A on the equilibrium phase diagram in Fig. 3. Evolution of the order parameter shows fast oscillations which decay in the long-time limit. The evolution of the average number of

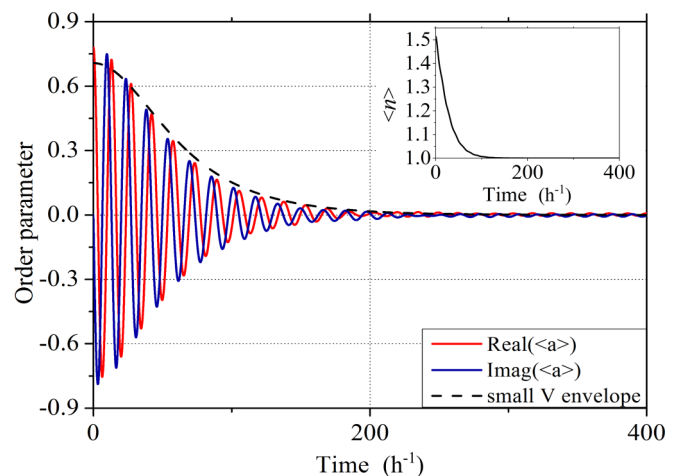


FIG. 4. Time evolution of the local order parameter $\langle a(t) \rangle$, real and imaginary parts, after the quench of the local energy on the impurity site from the IBEC to the IMI phase with $\langle n \rangle = 1$. Parameters of the quench are $\epsilon_0(t = 0) = -1$ and $\epsilon_0(t > 0) = -0.5$ at fixed coupling $V = 0.447$ (this quench protocol is schematically depicted with the arrow A in Fig. 3). Dashed line shows the envelope calculated analytically in the weak-coupling limit using Eq. (16). Time evolution of the average number of particles per mode at the impurity site $\langle n(t) \rangle$ for the same quench parameters is shown in the inset.

particles at the impurity $\langle n(t) \rangle$ is shown in the inset in Fig. 4. The average number of particles decays to the expectation value defined by the final Hamiltonian.

The fast oscillatory behavior of the order parameter is related to the internal impurity dynamics. The impurity Hamiltonian (2) after the quench of the local energy on the impurity site to the value $\varepsilon_0 = -0.5$ has an energy gap between the ground state and the first excited state equal to $E_{1,0} = 0.5$. The period of the fast oscillations of the order parameter roughly corresponds to $2\pi/E_{1,0} \approx 12.6$. The slight variation of the period of oscillations can be attributed to the effect of the lattice degrees of freedom on the impurity dynamics. The fast oscillations of the order parameter appear for all quenches when the coupling parameter is small, $V^2/(Uh) \lesssim 0.4$.

The time scale associated with the slow decay is calculated analytically in the limit of the weak coupling and is shown in Fig. 4. It shows good qualitative agreement and its derivation is shown in Sec. IV A.

IMI-IMI quench. The evolution of the local order parameter after the quench between two IMI phases (quench protocol B) with different number of particles at the impurity site is considered. In the initial IMI state, the equilibrium value of the order parameter is zero, $\langle a(t=0) \rangle = 0$. Such a state is a fixed point of Eqs. (4), (7), and (9). To allow the nontrivial dynamics of the order parameter $\langle a(t) \rangle$ starting from the IMI phase a small deviation of the order parameter from its vanishing equilibrium value is assumed, $\langle a(t=0) \rangle = \delta a$. We call the value δa as a seed noise. The presence of symmetry-breaking fluctuations slightly shifts the system away from its unstable fixed point and allows for the transition between two symmetric phases.

Figure 5 shows the post-quench evolution of the local order parameter. After the quench, the order parameter grows

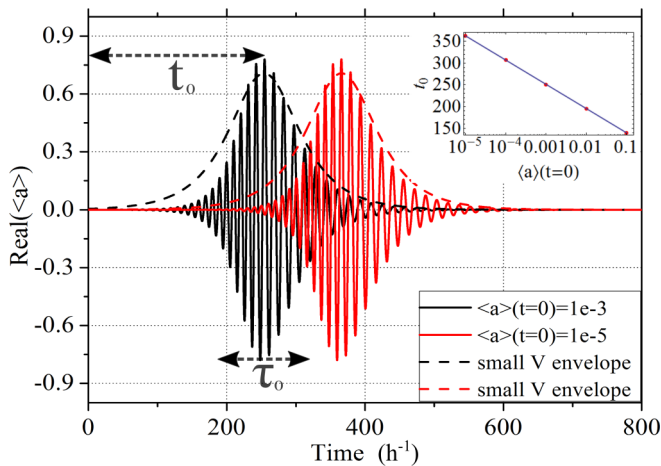


FIG. 5. Time evolution of the real part of the local order parameter $\langle a(t) \rangle$ after the quench of the local energy on the impurity site from IMI phase with $\langle n \rangle = 2$ to IMI phase with $\langle n \rangle = 1$ is shown for different values of the initial seed noise $\langle a(0) \rangle$. Parameters of the quench are $\varepsilon_0(t=0) = -1.5$ and $\varepsilon_0(t > 0) = -0.5$ with $V = 0.447$ (this quench protocol is schematically depicted with the arrow B in Fig. 3). The lifetime of the intermediate phase is τ_0 . Dashed line shows the envelope calculated analytically in the weak-coupling limit using Eq. (16). The inset shows the dependence of the response time t_0 on the initial seed noise amplitude $\langle a(0) \rangle$.

from its initial value defined by the seed noise δa . Similar to the IBEC-IMI transition, the period of fast oscillations of the order parameter is determined by energy differences of the isolated impurity Hamiltonian. At certain time t_0 the amplitude of oscillations reaches its maximum. This time decreases with the amplitude of the seed noise as $t_0 \propto -\ln(\delta a)$; the numerical result is shown in the inset in Fig. 5. After the maximal amplitude is reached, the oscillations decay. Finally, the new ground state is approached and the average number of particles saturates at the value defined by the phase of the final Hamiltonian. In this way, the system undergoes a transition between IMI lobes with different number of particles through a transient IBEC phase.

In Sec. IV A, we show that the observed relaxation to the IMI state can be described analytically assuming a weak coupling between the impurity and the lattice. Such an approach provides a good estimation for the envelopes of the time dependence of the order parameter. Their “slow” time scale τ_0 is determined by the coupling constant and the density of the lattice states.

C. Quenches to IBEC phase

IMI-IBEC quench. We now consider a quench from the IMI phase to the IBEC phase. Time evolution of the order parameter after the quench of the local energy is presented in Fig. 6. Parameters of this quench are schematically depicted with arrow C on the equilibrium phase diagram in Fig. 3. As in the case for IMI-IMI quench, the initial state is an unstable stationary point of the equations of motion of the order parameter. A small seed noise has been introduced into the initial conditions to allow a nontrivial dynamics of the order parameter with possible transition between the two phases. At short times, there is a rapid increase of the amplitude of the

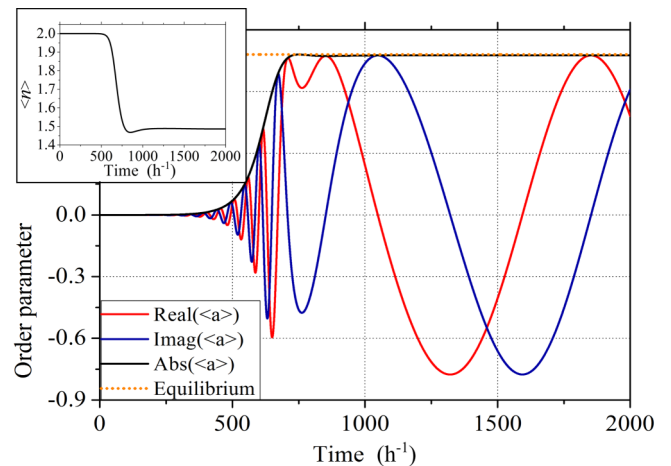


FIG. 6. Evolution of the local order parameter $\langle a(t) \rangle$ (its real and imaginary parts, as well as its absolute value) after the quench of the local energy on the impurity site from the IMI phase with $\langle n \rangle = 2$ to the IBEC phase is shown. Parameters of the quench are $\varepsilon_0(t=0) = -1.5$ and $\varepsilon_0(t > 0) = -1$ with $V = 0.447$ (this quench protocol is schematically depicted with the arrow C in Fig. 3). Expectation value of the order parameter in the ground state of the final Hamiltonian is shown with the dashed line. Inset shows the evolution of the average number of particles at the impurity site $\langle n(t) \rangle$.

order-parameter oscillations. The amplitude saturates after a time period dependent on the initial seed noise amplitude, similar to IMI to IMI quench considered above. For longer times, the phase of the order parameter rotates persistently and the order parameter never reaches its steady state. The number of particles at the impurity site decreases from the quantized initial value and saturates to the new equilibrium value (see inset in Fig. 6). Calculations for various initial values of the seed noise show that the persistent oscillations of the order parameter are the robust feature of the system, although the period of the oscillations varies with the particular choice of the seed noise.

The phase of the order parameter shows nontrivial features in its dynamics. The order-parameter vector rotates on the complex plane clockwise up to certain moment when the direction of the rotation changes to the counterclockwise one. This means that the rotation frequency interpolates between a positive value for short times and negative constant value for asymptotically large times. For the dynamics shown in Fig. 6, the transition between the two regimes takes place around $t \simeq 750$.

IBEC-IBEC quench. We consider the quenches of the local energy when the parameters of the initial and final Hamiltonians are chosen to correspond to the system in the IBEC phase. On the equilibrium phase diagram we depict these quenches as D, E, and F (see Fig. 3). There are two distinct cases: (i) quenches within the IBEC phase without crossing any IMI lobe (e.g., quenches D in Fig. 3) and (ii) quenches that cross at least one IMI lobe, e.g., quenches E and F in Fig. 3 cross one IMI lobe or two IMI lobes correspondingly.

First, let us consider the quenches that do not cross any IMI lobe. We fix the final value of the local energy $\varepsilon_0(t > 0)$ and vary the quench amplitudes $\Delta\varepsilon_0 = -[\varepsilon_0(t = 0) - \varepsilon_0(t > 0)]$ by setting the initial condition. As an example, we consider a set of quenches depicted with D arrows in Fig. 3. The post-quench time evolution of the real part of the order parameter is shown in Fig. 7. For small values of the quench amplitude $\Delta\varepsilon_0$, the order parameter approaches the new equilibrium value defined by the expectation value in the ground state of the final Hamiltonian. As $\Delta\varepsilon_0$ increases, the long-time evolution of the order parameter changes qualitatively from the relaxation to an oscillatory regime. A critical value of the quenching amplitude $\Delta\varepsilon_0^{\text{crit}} \simeq 0.8719$ separates these two very distinct regimes. At this singular point, the solution is neither oscillating nor reaching its static equilibrium value. As small deviations to this value lead to different asymptotic dynamical phases, we will refer to this singular point as a *dynamical phase transition*. Our numerical calculations show that the different asymptotic behavior is observed within the very small range of the quenching amplitudes close to the critical quench value, namely, for $\Delta\varepsilon_0 = \Delta\varepsilon_0^{\text{crit}} \pm 10^{-4}$. This gives an evidence that we observe a true dynamical transition. Note that in the oscillatory regime both the amplitude and the frequency of the oscillations depend on $\Delta\varepsilon_0$. As $\Delta\varepsilon_0$ tends to the critical value, the amplitude approaches the equilibrium static value and the frequency vanishes. For different final points of $\varepsilon_0(t > 0)$, our results (not shown) also demonstrate the presence of a dynamical transition. However, the critical value of the quench amplitude $\Delta\varepsilon_0$ is different and the critical amplitude increases with $-\varepsilon_0(t > 0)$ and V . Indeed, the dynamical transition

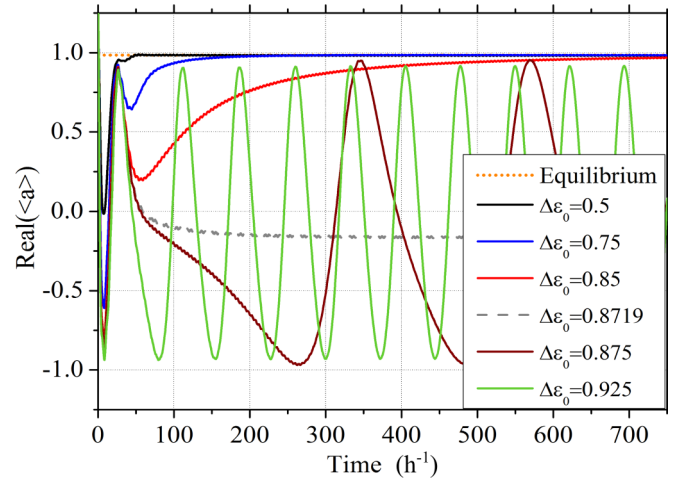


FIG. 7. Time evolution of the real part of order parameter for quenches within the IBEC phase for different quench amplitudes $\Delta\varepsilon_0 = -[\varepsilon_0(t = 0) - \varepsilon_0(t > 0)]$ for the same final value of the local energy $\varepsilon_0(t > 0) = -1$ when interaction strength is fixed $V = 0.89$ (these quenches are depicted with arrows D in Fig. 3). There are two distinct behaviors in the long-time regime: (i) an equilibrated static steady state for small values of $\Delta\varepsilon_0$ and (ii) an oscillatory regime with frequency and amplitude that depend on $\Delta\varepsilon_0$. Expectation value of the order parameter in the ground state of the final Hamiltonian is shown with the dashed line.

can most easily be observed near the IMI-to-IBEC transition line.

Finally, we consider quenches within the IBEC phase that cross one or more IMI lobes, depicted with the arrows E1 and F in Fig. 3. To highlight features of IMI lobe crossing observed in the evolution of the order parameter, we compare case E1 with the quenches with the same initial and final values of the local energy and different value of the coupling strength V such that no lobe is crossed (cases E2 and E3 in Fig. 3). Figure 8 shows the time evolution of the real part of the order parameter and the average number of particles $\langle n(t) \rangle$ for the three values of coupling strength V . For the lobe crossing case, $V = 0.316$, there is a plateau in the time evolution of the number of particles which corresponds to $\langle n \rangle \simeq 2$; this is the value of $\langle n \rangle$ of the IMI lobe crossed. In the long-time limit, the new equilibrium value is reached, defined by the final Hamiltonian. When the interaction strength V is large and no IMI lobe is crossed, there are two effects: first, the long-lived transient phase is lost, and second, for sufficiently large interactions V , a dynamical phase transition to an oscillatory phase takes place. The latter behavior is similar to the one shown in Fig. 7.

The existence of a plateau with $\langle n \rangle \simeq 2$ suggests that the long-lived transient phase acquires characteristic features of the crossed IMI phase. The phenomenon of the locking of the particle number at an integer value whenever the corresponding IMI lobe is crossed is ubiquitous for this model. Figure 9 shows evolution of the number of particles and of the order parameter after a quench crossing two IMI lobes. Two long-lived plateaus are observed in $\langle n \rangle(t)$ around $\langle n \rangle \simeq 2$ and 1 before the final relaxation to the local equilibrium value occurs. Within each plateau the amplitude of the oscillations of $\langle a \rangle$ is

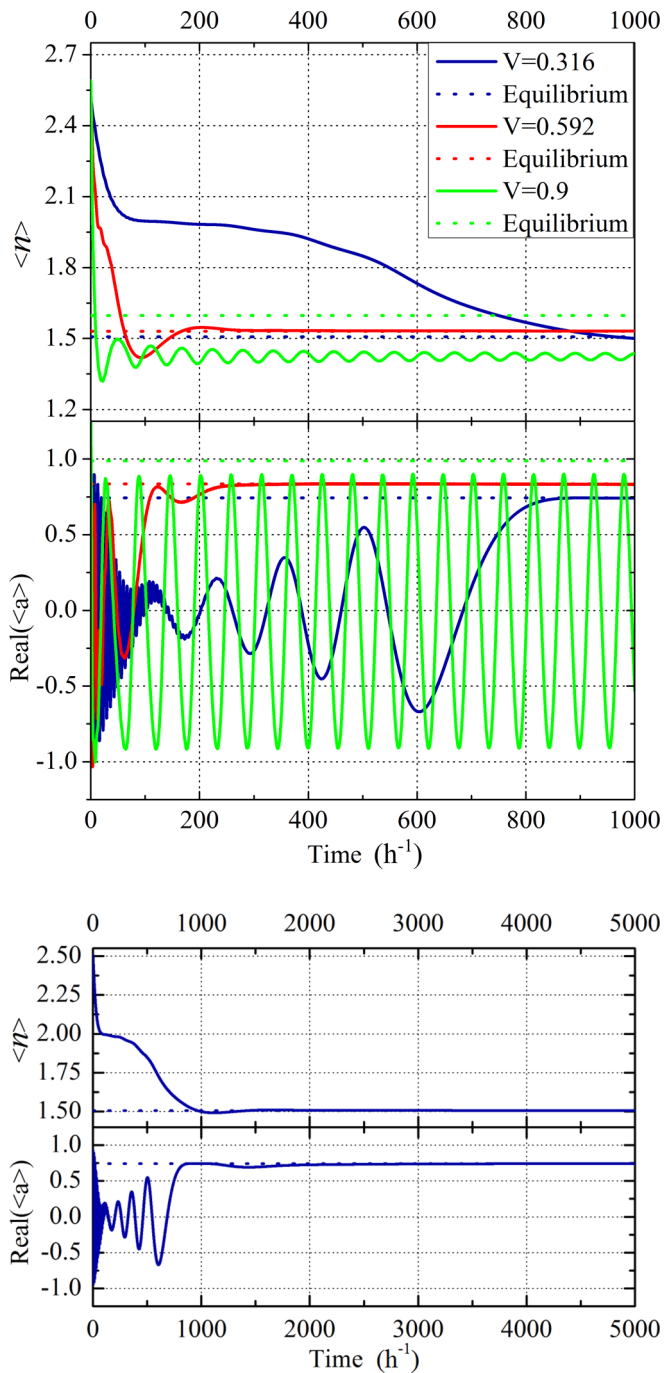


FIG. 8. Time evolution of the real part of the order parameter (upper panel) and number of particles on the impurity site $\langle n \rangle(t)$ (middle panel) for fixed initial and final values of the local energy $\varepsilon_0(t=0) = -2$ and $\varepsilon_0(t > 0) = -1$ correspondingly and three values of the coupling strength: $V = 0.316, 0.592, \text{ and } 0.9$. These quenches are depicted with arrows E1–E3 in Fig. 3. Dotted lines correspond to the expectation values $\langle a \rangle$ and $\langle n \rangle$ calculated in the ground state of the final Hamiltonian. A plateau can be observed in the time evolution of the $\langle n \rangle$ corresponding to $\langle n \rangle = 2$ in the case when IMI phases crossed during the quench. The long-time behavior of the order parameter and number of particles for the quench with $V = 0.316$ is shown in the lower panel.

small. In this way, the system seems to mimic a vanishing order parameter during these long-lived transient phases.

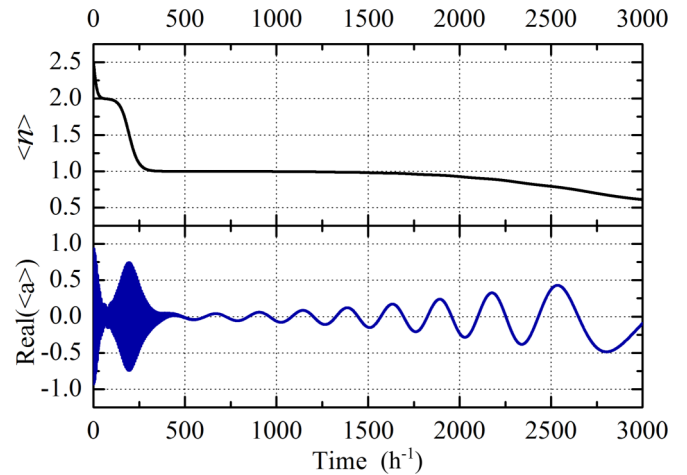


FIG. 9. Time evolution of the real part of order parameter (down) and of number of particles (up) for the quench, depicted with arrow F, which crosses two Mott lobes: $\varepsilon_0(t=0) = -2, \varepsilon_0(t > 0) = 0$ at $V = 0.316$.

D. Inverse quenches

For all the quenches shown in Fig. 3 and described above the number of particles at the impurity site decreases with time with respect to its initial value. This process is always possible since there is an infinite number of bath modes to which particles can be emitted. We also considered quenches for which the equilibrium state of the final phase contains a larger number of particles at the impurity than the initial state does. It corresponds to the inversion of the direction of arrows in Fig. 3. Local equilibration is in this case never achieved as the bath effectively decouples. Indeed, the Hamiltonian (1) conserves total number of particles in the system. Bulk of the lattice contains no particles at the initial state of the system, therefore, the bath is not able to provide extra particles for the impurity to achieve its local equilibrium state. For completeness, we provide a description of the time evolution in this case. When starting from IMI the system seems to be locked in its initial phase: the order-parameter amplitude undergoes an oscillatory motion with an amplitude that never exceeds the initially introduced seed noise. Thus, contrarily to the previous case, the initial state is stable and the system never leaves the initial IMI phase. When starting from IBEC phase, the long-time behavior is always oscillatory even for very small quench amplitudes. We have also verified numerically that quenches with zero amplitude do not change a state of the system, even in the presence of the seed noise.

IV. DISCUSSION

A. Transient phases

An interesting and striking feature of the post-quench dynamics is the appearance of long-lived transient regimes, when an equilibrium phase is crossed, with the same characteristics of an underlying phase. We dubbed such regime a transient phase.

A transient IBEC phase can be observed during the transition regime between IMI lobes in the IMI to IMI quenches of Fig. 5. During this regime, the order parameter becomes

finite and the number of particles fluctuates. The phenomenon is even more striking in IBEC to IBEC quenches that cross one of more IMI lobes. The long plateaus observed at integer values in the dynamics of $\langle n \rangle(t)$ (see Fig. 8) can be interpreted as the formation of transient IMI phases.

A simple physical picture capturing the main features of IMI to IMI quenches can be obtained in the limit of small V . This regime is usually considered in quantum optics, where atoms in excited states are coupled to the electromagnetic continuum [58]. Here, we adapt the standard argument for the calculation of the super-radiance intensity to our system. For clarity, we consider only IMI to IMI transitions between phases with $n + 1$ and n particles. The weak coupling formally corresponds to a small value of V and, consequently, of λ . We thus consider a perturbative series in this parameter.

At zeroth order, the bath is in its vacuum state $|0_{\text{bath}}\rangle$, and the wave function of an impurity is considered to be in a symmetric state with each mode in a superposition of n and $n + 1$ particles:

$$|\Psi^{(0)}\rangle = |0_{\text{bath}}\rangle \otimes_{j=1}^N (\phi_n |n\rangle_j + \phi_{n+1} |n+1\rangle_j). \quad (11)$$

After a time T the first-order correction, corresponding to the irradiation of a particle to the bath, is given by the formula

$$|\Psi^{(1)}\rangle = \sum_{jk} b_k^\dagger \tilde{a}_j \int_0^T e^{-i(\epsilon_k - \epsilon_{n+1} + \epsilon_n)t} dt |\Psi^{(0)}\rangle. \quad (12)$$

Here, $\tilde{a} = PaP$ is the annihilation operator projected into the considered subspace with $P = |n+1\rangle\langle n+1| + |n\rangle\langle n|$ and ϵ_n is the energy of the impurity Hamiltonian with n particles. The overall transition rate equals $W = \partial_T \langle \Psi^{(1)} | \Psi^{(1)} \rangle$. Taking the $T \rightarrow \infty$ limit we can write $W = \lim_{T \rightarrow \infty} T^{-1} \langle \Psi^{(1)} | \Psi^{(1)} \rangle$. Calculating the averages

$$\begin{aligned} \langle \Psi^{(0)} | \tilde{a}_j^\dagger \tilde{a}_j | \Psi^{(0)} \rangle &= (n+1) |\phi_{n+1}|^2, \\ \langle \Psi^{(0)} | \tilde{a}_j^\dagger \tilde{a}_{j'} | \Psi^{(0)} \rangle &= (n+1) \phi_n \phi_{n+1}, \quad j' \neq j \end{aligned} \quad (13)$$

we obtain

$$W = 2\pi(n+1)V^2 A_{\epsilon_{n+1}-\epsilon_n} (|\phi_{n+1}|^2 + (N-1)\phi_n \phi_{n+1}), \quad (14)$$

where $A_{\epsilon_{n+1}-\epsilon_n}$ is the normalized density of lattice states at the transition energy. The first term in the parentheses describes the spontaneous emission yielding Fermi's golden rule. In the large- N limit, the contribution of this term is small. The second term describes the super-radiance of synchronized impurity modes.

The quantity W can be interpreted as a decay rate of the population of the state $|n+1\rangle$. In the large- N limit, we can thus write $W = N \frac{d|\phi_{n+1}|^2}{dt}$, which yields the detailed balance equation

$$\left. \frac{d|\phi_{n+1}|^2}{dt} \right|_{N \rightarrow \infty} = -\frac{|\phi_{n+1}|^2(1 - |\phi_{n+1}|^2)}{\tau_0}. \quad (15)$$

Here, we introduced the time scale $\tau_0^{-1} = 2\pi(n+1)V^2 A_{\epsilon_{n+1}-\epsilon_n}$ and took into account the normalization condition $|\phi_n|^2 + |\phi_{n+1}|^2 = 1$. Solving the differential equation (15), we obtain the envelope of the order parameter

in the weak-coupling limit:

$$\langle a \rangle(t) = \sqrt{\frac{n+1}{2 + 2\text{ch}(t-t_0)/\tau_0}}, \quad (16)$$

where t_0 is fixed by the initial condition. The instant-onlike envelope functions obtained in this way are depicted in Fig. 5 and are in good agreement with the numerical results. The logarithmic dependence of t_0 on δa , shown in the inset of Fig. 5, also arises from Eq. (16).

A similar argument could be made for IBEC to IBEC quenches at small V , shown in Fig. 8. Since three states $|n-1\rangle, |n\rangle, |n+1\rangle$ are involved in the process, a simple analytical solution could not be found. Nonetheless, we can use the previous case to argue that this process can be seen as two half-instantonlike solutions. After the quench, the impurities relax from the mixed state $\phi_3|3\rangle + \phi_2|2\rangle$ with approximately equal $\phi_{2,3}$. This stage of the evolution at $t \approx 100$ yields almost a pure IMI $n = 2$ state; the value of order parameter is decreased considerably. However, this transient IMI phase is not stable and decays to IBEC. The period of the long-time oscillations of the order parameter seems to vary with time, suggesting an intricate interplay of degrees of freedom in the course of the evolution.

In this paper, we limit our study to the $N \rightarrow \infty$ case. Nonetheless, possible realizations of the generalized multi-component Bose-Anderson Hamiltonian forcefully feature a finite number of modes. Thus, we now discuss experimentally relevant finite- N effects. Qualitatively, two relaxation mechanisms are possible, as can be seen from Eq. (14): the collective super-radiance, discussed above, and a set of independent spontaneous emission processes. The latter are characterized by the single-particle lifetime $t_{sp} = \tau_0 N$, that is N times larger than the lifetime due to super-radiant processes. Consequently, the relative impact of spontaneous emission processes can be roughly estimated as $2|\ln(\delta a)|/N$. This allows a lower bound on N (given the seed noise value δa) above which spontaneous emission processes can be ignored. On the other hand, given the number of components N , this estimation allows to put a lower bound for the seed noise value. Therefore, it is as if a certain amount of quantum noise is intrinsically present in the system. External sources of noise, such as interactions with the surroundings, finite temperature, etc., can only increase this value. Note that this is indeed a rough estimation since Eq. (14) is obtained by perturbative arguments.

For adiabatic processes, the state of the systems under evolution follows the instantaneous ground state. Therefore, if changes to the Hamiltonian are performed adiabatically, say along the arrows E1 or F, the appearance of a transient phase during the crossing of a foreigner equilibrium phase is to be expected. In contrast, for the sudden quenches we address here, the parameters of the Hamiltonian are instantaneously switched from the start to the end point of the arrows in Fig. 3, never taking values belonging to the equilibrium phase along the way. These facts render even more surprising the appearance of the long-lived transients observed here for which the quenched dynamics qualitatively resembles the adiabatic one. Note, however, that whereas the adiabatic state of the system is fully characterized by its wave function, the dynamical equations (4), (7), and (9) have a memory kernel.

Thus, an instantaneous state of the system during its evolution is characterized by its wave function as well as by the previous time dependence of the order parameter $\langle a(t) \rangle$.

B. Dynamical phase transition

Another remarkable feature of the post-quench dynamics is the dynamical phase transition, arising for quenches deep in the IBEC phase. As described in Sec. III C, a critical value of the quench amplitude $\Delta\varepsilon_0$ could be found that separates a fully relaxed long-time state from a regime where the system remains with an excited state. The latter case is characterized by a persistent phase rotation of $\langle a \rangle$, whereas its modulus approaches a constant value, and is observed for a quench amplitude larger than the threshold amplitude. We did not observe any damping for the time scales available in our calculations, including for quenches very close to $\Delta\varepsilon_0^{\text{crit}}$. The presence of a well-defined critical quench amplitude $\Delta\varepsilon_0^{\text{crit}}$ where the behavior of the system changes qualitatively is a strong evidence of a dynamical phase transition. Mathematically, it corresponds to a nonanalytical dependence of the final asymptotic state on the quench strength.

To explain the nature of the frictionless phase rotation, let us consider the possible relaxation mechanisms. According to Eq. (7), energy and, therefore, particles transfer from the impurity to the lattice mode k whenever $\langle a(t) \rangle$ contains a nonzero Fourier component at frequency ε_k . Assuming, for the sake of the argument, that $\langle a \rangle = a_0 e^{-i\varepsilon_k t}$, the solution of Eq. (7) reads as $\beta_k(t) = [V_k \sqrt{N} a_0 t + \beta_k(0)] e^{-i\varepsilon_k t}$, corresponding to a linear-in-time increase of the amplitude of the k mode. This argument is only valid for short times before nonlinear effects ensue. Nonetheless, it provides a physical picture for the energy transfer between the impurity and the lattice with depletion of the Fourier component $\omega = \varepsilon_k$ in the oscillatory behavior of $\langle a(t) \rangle$. Since lattice oscillators form a continuum spectrum for $\omega > 0$, the only possibility for a frictionless dynamics is the existence of some spectral weight of $\langle a(t) \rangle$ in the negative frequencies. In this case, the order parameter effectively decouples from the continuum of single-particle lattice excitations. This simple picture is confirmed by our observations. Figure 6 shows that the order parameter $\langle a \rangle$ rotates clockwise on the complex plane at the initial stages of evolution, and afterwards the rotation suddenly changes to counterclockwise direction. In this case, most of the spectral weight belongs to the negative frequencies. A small part contributing positive frequencies reveals itself in the amplitude oscillations of the order parameter. The latter are dissipative, so that finally a pure phase rotation $\langle a \rangle = a_0 e^{i\omega t}$ with $\omega > 0$ is observed. The same counterclockwise rotation occurs after the quenches within IBEC phase as it can be seen from Fig. 7 and from the Husimi function plot of the same data, presented in Fig. 1.

The negative part of the spectrum appears to correspond to states with less particles than the equilibrium one. A simple explanation can be given as follows. Consider a single-impurity Hamiltonian (2) with some $\varepsilon_0 < 0$, $U > 0$. It has a nonmonotonous spectrum: the energy E_n decreases with the number of particles n until n reaches the equilibrium value $n_0 \approx -\frac{\varepsilon_0}{U} - \frac{1}{2}$. The counterclockwise phase rotation is realized for a superposition state $|\Psi\rangle = \alpha e^{-iE_n t} |n\rangle +$

$e^{-iE_{n+1} t} \beta |n+1\rangle$ if $E_n < E_{n+1}$, that corresponds to $n, n+1$ being less than the equilibrium number of particles n_0 .

The asymptotic long-time dynamics of the impurity model (1) is determined by the number of bosons N_∞ contributing the IBEC at $t \rightarrow \infty$. In N_∞ we count the particles on the impurity itself, as well as in the IBEC cloud located near the impurity and interacting with it. However, N_∞ does not include all the particles of the system. As we discussed above, the relaxation processes take place at the initial stages of evolution, and the relaxation is associated with the emission of particles from the IBEC cloud, the particles of which run away from the impurity and cannot be absorbed back to the cloud. A partial runaway of bosons is obvious for the quench between the IMI phases with $\langle n \rangle = 2$ and 1 (remind that the lattice modes are not polarized in the IMI phase, so that N_∞ has contributions only from bosons on the impurity). We conclude that the phase-rotating states obey a smaller N_∞ than the equilibrium one. As the collective IBEC state contains a large amount of bosons, a gradual change of N_∞ gives rise to a continuous spectrum of the rotation frequency: smaller number of particles corresponds to faster rotation.

While the total number of particles in the system is conserved, the value of N_∞ particularly depends on the emission dynamics. A dynamical phase transition separating the evolution towards the new equilibrium and the permanent phase-rotating state provides an evidence that emission of particles during the after-quench evolution is essentially nonadiabatic. After the quench with a large amplitude, the system emits more particles than it is required to reach the new equilibrium state. Since the emitted particles cannot be absorbed back to the IBEC, such an ‘‘overshooting’’ results in persistent phase rotation, as Fig. 10 illustrates. The smaller the quench amplitude is, the larger number of particles remains in the system and the faster phase oscillations are. Below the critical quench amplitude, the ‘‘overshooting’’ is absent.

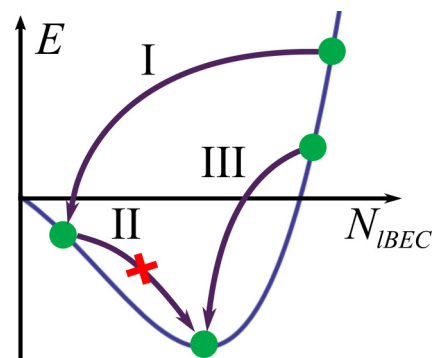


FIG. 10. The illustration of how the persistent oscillating phase appears. The transition I corresponds to the quench within the IBEC phase with large quench amplitude (D series in the Fig. 3). During the nonadiabatic evolution I, the impurity loses more particles than it is required to reach the ground state. Once the state with the minimal energy is ‘‘overshot’’, it cannot be reached because emitted particles never return to the impurity (that is, the transition II is forbidden). Transition III corresponds to the D series quench with an amplitude below the critical value. In this case, the evolution is more adiabaticlike, and the system relaxes to the ground state.

The existence of a persistent rotating phase can also be seen as a symmetry-broken ground state of a Hamiltonian in a convenient rotating frame. The change of frame corresponds to the gauge transformation $\tilde{a} = ae^{i\omega t}$, $\tilde{b}_k = b_k e^{i\omega t}$, so that $\langle \tilde{a} \rangle$ becomes time independent for asymptotically long times. The gauge transformation introduces an effective chemical potential:

$$H^\omega = \sum_j (\varepsilon_0 + \omega) a_j^\dagger a_j + \frac{U}{2} \sum_j a_j^\dagger a_j^\dagger a_j a_j - \sum_{j,k} \frac{V_k}{\sqrt{N}} (a_j^\dagger b_k + \text{H.c.}) + \sum_k (\varepsilon_k + \omega) b_k^\dagger b_k. \quad (17)$$

For this Hamiltonian, the existence of a symmetry-broken ground state with nonvanishing $\langle \tilde{a} \rangle$ corresponds to a persistent phase rotation in the original frame. These considerations imply that a finite gap in the bath spectrum ε_k , as well as a shift in ε_0 , would only shift the value of ω for which the symmetry-broken phase starts to appear. Therefore, the undamped oscillatory phase is expected generically for quenches within IBEC phase.

An analysis of the Hamiltonian (17) also gives more insight about the nature of the dynamic transition. The remarkable consequence of the energy gap appeared in (17) is that expression for the number of particles in the lattice cloud $\sum_k \langle b_k^\dagger b_k \rangle = N \sum_k V_k^2 \frac{|a|^2}{(\varepsilon_k + \omega)^2}$ is not divergent at small k for $\omega > 0$, in contrast to the case of the gapless reservoir in (1). Therefore, the number of particles in the persistent rotating phase is not just quantitatively smaller than for IBEC; the difference is qualitative. We also conclude that the observed scenario of the dynamic transition cannot be realized (or at least requires a major modification) for higher dimensions $d > 4$ since in that case, the sum converges for a gapless reservoir as well.

Let us discuss the nature of the IBEC phase, in view of these findings. Strictly speaking, calling this phase a superfluid is not well justified, as there is no evidence of superfluid dynamics in the Bose-Anderson impurity model. Even the persistent rotating phase also does not imply a flow of particles. Here, a continuous spectrum of frictionless excitations can be seen as reminiscent of the superfluidity in a zero-dimensional system.

Now, we address the consequences of our findings for the existence of a frictionless phase-rotation regime in the finite- N case. We concluded that for $N \rightarrow \infty$ the dynamical transition separates the IBEC phase and persistent rotating phase, respectively, containing an infinite and a finite number of particles in the cloud. An infinite number of particles in the IBEC mode was also found for the single-component Bose-Anderson impurity model [24]. Moreover, a narrow peak at negative frequencies has been observed in the equilibrium local spectral function of the zero-temperature single-component Bose-Anderson impurity model [24]. Both $N = 1$ and $N \rightarrow \infty$ cases share this feature, with a major part of the spectral weight belonging to the positive semiaxis. We interpret this peak as evidence that $N = 1$ model has the excitations analogous to the rotating-phase state. Of course, the presented argumentation does not prove that the dynamic transition we found for $N \rightarrow \infty$ also shows up for a finite N . There can be at least two other possibilities. First, it might

happen that a critical quench value vanishes for a finite N , so that the system can never relax to the new equilibrium state. In this case, no dynamic transition will be realized. Second, it is not clear if the symmetry-broken state is stable for a finite ω , or the rotating state will decay to $\langle a \rangle = 0$ because of quantum fluctuations in a finite- N system. In the latter case, the dynamic transition will take the place, but its properties will be different from the $N = \infty$ system. Solving these questions will be a subject of the future work.

Finally, let us address the differences and similarities of the persistent rotation phase found here with that found in the dynamics of the superconducting order parameter in the BCS model [14]. Depending on the initial quench, the BCS system can also show a relaxation to the new steady state or persistent oscillations of the order parameter. There are, however, remarkable differences from the case studied here: (i) In the B-SIAM, interactions and quenches are local, therefore, the energy injected to the system is not extensive and, as a consequence, the relaxation to the new equilibrium ground state is to be expected. On the contrary, in the BCS case the system never relaxes to the ground state but rather to a finite-energy state. (ii) The analysis of the BCS model [14] is based on its mapping to a classical dynamical system within Anderson pseudospin representation. Furthermore, integrability is exploited. In our case, the impurity part of the Hamiltonian is treated exactly and the integrals of motion can hardly be established. (iii) As a result of the mean-field treatment in the BCS case, the system is effectively Gaussian. In our case, local interactions are treated exactly and are highly non-Gaussian. (iv) Finally, as discussed above, our system is robust against $1/N$ corrections whereas in the BCS phase the possible effect of anharmonic corrections terms is not clear.

V. CONCLUSIONS

We have studied quenches in the N -component Bose-Anderson model, which in the $N \rightarrow \infty$ limit allows a numerically exact solution. Such treatment is possible because the $N \rightarrow \infty$ limit corresponds to the suppression of quantum fluctuation of the bath degrees of freedom rendering exact a mean-field-like treatment of the bath modes. As local interaction effects are kept at the impurity level, our approach is able to capture a set of interesting phenomena arising due to quantum many-body correlations. The model exhibits a rich set of dynamical regimes at different time scales as a result of the interplay between local and bath degrees of freedom: short times are related with the internal impurity degrees of freedom, whereas the long-time dynamics is determined by the collective modes.

The equilibrium zero-temperature phase diagram of the B-SIAM consists of a set of IMI lobes and a IBEC phase. This nontrivial phase diagram allows for IMI-IMI or IBEC-IBEC quenches that cross the complementary phase. These quenches are observed to give rise to long-lived transient phases. The transient IBEC-like phase, formed while quenching between the IMI states, is explained using analytic consideration valid for a weak bath-impurity coupling. A parallel is drawn with the super-radiant regime arising in the celebrated Dicke model [59], which describes a large number of two-level systems

interacting with a bosonic field. Long-lived IMI-like plateaus are found for IBEC-to-IBEC quenches that cross Mott lobes.

A nondecaying mode is found throughout IBEC phase. This negative frequency excitation is well separated from the spectral continuum located at positive energies. The existence of such long-lived mode ensures the possibility of observing persistent phase rotations of the order parameter for quenches with a large enough amplitude. As its characteristic frequency is negative, the phase of the order parameter rotates counterclockwise, whereas all clockwise rotating, i.e., positive energy, modes are damped due to the interaction with the bath degrees of freedom. The nondecaying mode is unique and corresponds to a well-defined frequency at each point of the phase space of the model. The particular value of the frequency depends on the total particle number. This fact, together with the conservation of particle number throughout the evolution that is fixed by the initial state, explains that quenches to the same point in phase space give rise to persistent oscillations with different frequencies.

A dynamical phase transition is found, as a function of the quench amplitude, separating the regimes where the evolution either attains the equilibrium IBEC phase or retains a persistent oscillating phase. The high accuracy of the calculations has allowed us to obtain strong numerical evidence that the two regimes are separated by a singular line, so that a true dynamical transition, rather than a crossover, occurs.

Our findings, regarding the existence of a persistent phase-rotation mode, are robust to $1/N$ corrections and should be present down to $N = 1$ since a resonance at negative energies has already been reported in the spectral function of the B-SIAM [24]. This phenomenon is generic and should be observed ubiquitously in open quantum systems whenever conservation laws permit the existence of isolated spectral modes.

More general implication of the work will require a consideration of the several impurities connected to the different lattice sites. The main difference of these systems from that considered in our work is that their finite size makes the persistent (superfluid) current possible. Thus, they can be considered as (quantum) memory cells and their relaxation dynamics becomes of potential technological importance.

ACKNOWLEDGMENTS

We acknowledge useful discussions with P. I. Arseev, I. S. Krivenko, G. Rohringer, and V. I. Yudson. P.R. acknowledges financial support from FCT through the contract Ref. No. IF/00347/2014/CP1214/CT0002 under the IF2014 program. D.V.C., Y.E.S., and A.N.R. thank the Dynasty foundation and RFBR (Grants No. 14-02-01219 and No. 16-32-00554) for financial support. Modeling of the quenches to IMI phase (Sec. II B) and the analysis of the transient phases (Sec. IV A) was funded by the Russian Science Foundation (RSF) Grant No. 16-42-01057.

APPENDIX: DYNAMICS IN THE LARGE- N LIMIT

1. Diagrammatics

Let us construct a formal $1/N$ expansion. The lattice degrees of freedom can be integrated out of the initial

Hamiltonian (2), yielding the action

$$S = \sum S_{\text{SI}}[a_j^\dagger a_j] + \sum_j a_j^\dagger \Delta_{t-t'} \sum_{j'} a_{j't'}, \quad (\text{A1})$$

where S_{SI} is the single-impurity action corresponding to the Hamiltonian (2), and $\Delta_t = \frac{V_k}{\sqrt{N}}(i\partial_t - \varepsilon_k)^{-1} \frac{V_k}{\sqrt{N}}$ is the hybridization function reflecting the hopping and lattice dispersion properties; the integration over time arguments is assumed. According to Eq. (9), $\lambda_t = \int \Delta_{t-t'}(a_{t'})$, and therefore the action can be rewritten as

$$S = \sum S_{\text{SI}}^{\text{eff}}[a_j^\dagger a_j] + \sum_j \tilde{a}_{j_t}^\dagger \Delta_{t-t'} \sum_{j'} \tilde{a}_{j't'}, \quad (\text{A2})$$

where $S_{\text{SI}}^{\text{eff}}$ corresponds to the effective impurity Hamiltonian (4), and $\tilde{a}_j = a_j - \langle a_j \rangle$ describes the displacement of the impurity j from the mean value. Neglecting the hybridization term in this formula, one restores the mean-field theory presented above. The deviations from this result can be estimated considering the serial expansion in Δ . Let us formally integrate out all the impurities, except a single one labeled j_0 . In the zeroth order, the impurities are uncorrelated, and the result of such an integration is just

$$S_{\text{SI}}^{(0)}[a_{j_0}^\dagger, a_{j_0}] = S_{\text{SI}}^{\text{eff}}[a_{j_0}^\dagger, a_{j_0}]. \quad (\text{A3})$$

The first order is contributed only by the diagonal term

$$S_{\text{SI}}^{(1)}[a_{j_0}^\dagger, a_{j_0}] = \tilde{a}_{j_0 t}^\dagger \Delta_{t-t'} \tilde{a}_{j_0 t'}. \quad (\text{A4})$$

The value of Δ scales as $1/N$, so the first-order correction is also proportional to $1/N$. The effect of mutual correlations between the different impurities arises in the second order. The second-order correction to the effective impurity action obeys the form

$$S_{\text{SI}}^{(2)}[a_j^\dagger, a_j] = \tilde{a}_{j_t}^\dagger \left(\sum_{j'} \Delta_{t-t_1} (\tilde{a}_{j't_1} \tilde{a}_{j't_2}^\dagger) \Delta_{t_2-t'} \right) \tilde{a}_{j't'}. \quad (\text{A5})$$

Since the averages $\langle \tilde{a}_{j'} \tilde{a}_{j''}^\dagger \rangle$ for $j' \neq j''$ are vanished in the zeroth order, they carry an additional smallness and should not be accounted in the right-hand side of (A5). The sum over j' contains N equal terms, so the entire expression scales as $1/N$. It is easy to see that higher expansion terms also carry $1/N$ prefactor. This concludes the proof that the mean-field theory is exact in the limit of infinite number of impurities.

2. Path integral

In this section, we derive the $1/N$ expansion and show that Eqs. (4) and (9) are exact in the large- N limit. We start by writing the generating function for the Hamiltonian (1) on the Keldysh contour γ :

$$Z[\xi] = \int \prod_j Da_j \prod_k Db_k e^{-i\{\sum_j S_j[\xi] + S_{\text{bath}} + S_{\text{int}}\}}, \quad (\text{A6})$$

where ξ 's are source fields and

$$S_{\text{loc},j}[\xi] = - \int dz dz' \sum_j a_j(z)^\dagger G_0^{-1}(z,z') a_j(z') \\ + \frac{1}{2} \int_\gamma dz \sum_j U(z) a_j^\dagger(z) a_j^\dagger(z) a_j(z) a_j(z) \\ - \int_\gamma dz \sum_j [\xi^\dagger(z) a_j(z) + a_j^\dagger(z) \xi(z)], \quad (\text{A7})$$

$$S_{\text{bath}} = - \int_\gamma dz \sum_k b_k^\dagger(z) g_k^{-1}(z,z') b_k(z'), \quad (\text{A8})$$

$$S_{\text{int}} = - \int_\gamma dz \sum_{k,j} \frac{V_k}{\sqrt{N}} [b_k^\dagger(z) a_j(z) + a_j^\dagger(z) b_k(z)] \quad (\text{A9})$$

are, respectively, the impurity, bath, and interaction terms in the action. G_0 and g_k are the propagators of the impurity and of the bath in the absence of coupling or interactions. Integrating out the bosonic bath one obtains an action solely in terms of the a fields

$$Z[\xi] = \int Da e^{-i(\sum_j S_{\text{loc},j}[\xi] + \frac{1}{N} \sum_{jj'} a_j^\dagger \Xi^{-1} a_{j'})}, \quad (\text{A10})$$

where

$$\Xi^{-1}(z,z') = \sum_k V_k(z) g_k(z,z') \bar{V}_k(z') \quad (\text{A11})$$

with $\Xi^\dagger = \Xi$. We now introduce a Hubbard-Stratonovich field λ to decouple the term in Ξ which factorizes the impurity action into independent components. Since the action is symmetric with respect to component exchange, the total action is N times the one of a single component. Therefore, we obtain

$$Z[\xi] = \int D\lambda e^{-iN S[\lambda]}, \quad (\text{A12})$$

where

$$S[\lambda] = - \int_\gamma dz dz' \lambda^\dagger(z) \Xi(z,z') \lambda(z') + F[\lambda], \quad (\text{A13})$$

$$F[\xi + \lambda] = i \ln \int Da e^{-i S_{\text{loc}}[\xi + \lambda]}. \quad (\text{A14})$$

Note that the fact that the action, in Eq. (A12), is multiplied by N makes the integral amenable to be treated by a saddle-point approximation whenever N is large.

We now proceed to derive the saddle-point conditions setting the sources ξ to zero. Varying the action in order to

λ^\dagger we obtain

$$\delta_{\lambda^\dagger(z)} S[\lambda] = - \int_\gamma dz' \Xi(z,z') \lambda(z') + \delta_{\lambda^\dagger(z)} F[\lambda]. \quad (\text{A15})$$

From the definition in Eq. (A14) we can identify $\delta_{\lambda^\dagger(z)} F[\lambda] = -\langle a(z) \rangle$, where the mean value $\langle \dots \rangle$ is taken with respect to the Hamiltonian (4). Setting the variation of the action to zero and inverting the kernel Ξ thus we obtain

$$\lambda(z) = - \int_\gamma dz' \Xi^{-1}(z,z') \langle a(z') \rangle. \quad (\text{A16})$$

In order to obtain the equations in the main text, we have to evaluate the former expression in the real-time branch of the Keldysh contour:

$$\lambda(t) = i \int_0^\beta d\tau \Xi^{-1\top}(t,\tau) \langle a(\tau) \rangle \\ - \int_0^t dt' [\Xi^{-1>}(t,t') - \Xi^{-1<}(t,t')] \langle a(t') \rangle. \quad (\text{A17})$$

Identifying the different components of Ξ , assuming the bath is at thermal equilibrium at $t = 0$ with inverse temperature β , we get

$$\Xi^{-1M}(\tau,\tau') = -i \sum_k V_k(0) \bar{V}_k(0) [n_b(\epsilon_k) + \Theta(\tau - \tau')] \\ \times e^{-\epsilon_k(\tau - \tau')}, \quad (\text{A18})$$

$$\Xi^{-1\top}(t,\tau') = -i \sum_k V_k(t) \bar{V}_k(0) n_b(\epsilon_k) e^{-i\epsilon_k(t+i\tau)}, \quad (\text{A19})$$

$$\Xi^{-1>}(t,t') = -i \sum_k V_k(t) \bar{V}_k(t') [n_b(\epsilon_k) + 1] e^{-i\epsilon_k(t-t')}, \quad (\text{A20})$$

$$\Xi^{-1<}(t,t') = -i \sum_k V_k(t) \bar{V}_k(t') n_b(\epsilon_k) e^{-i\epsilon_k(t-t')} \quad (\text{A21})$$

with n_b the Bose-Einstein distribution. With this assumptions, and using that along the thermal branch $\langle a(\tau) \rangle = \langle a(0) \rangle$, Eq. (A17) becomes

$$\lambda(t) = \sum_k V_k(t) \frac{e^{-it\epsilon_k}}{\epsilon_k} \bar{V}_k(0) \langle a(0) \rangle \\ + i \sum_k \int_0^t dt' V_k(t) e^{-i(t-t')\epsilon_k} \bar{V}_k(t') \langle a(t') \rangle, \quad (\text{A22})$$

which becomes Eq. (9) when V_k does not depend on time. In the limit $N \rightarrow \infty$, the saddle-point value of λ obtained by Eq. (A22) becomes exact.

-
- [1] D. Fausti, R. I. Tobey, N. Dean, S. Kaiser, A. Dienst, M. C. Hoffmann, S. Pyon, T. Takayama, H. Takagi, and A. Cavalleri, *Science* **331**, 189 (2011).
[2] M. Moeckel and S. Kehrein, *Phys. Rev. Lett.* **100**, 175702 (2008).
[3] C. Kollath, A. M. Läuchli, and E. Altman, *Phys. Rev. Lett.* **98**, 180601 (2007).

- [4] F. H. L. Essler, S. Kehrein, S. R. Manmana, and N. J. Robinson, *Phys. Rev. B* **89**, 165104 (2014).
[5] M. Babadi, E. Demler, and M. Knap, *Phys. Rev. X* **5**, 041005 (2015).
[6] P. Gagel, P. P. Orth, and J. Schmalian, *Phys. Rev. Lett.* **113**, 220401 (2014).
[7] T. Prosen and M. Znidaric, *Phys. Rev. B* **86**, 125118 (2012).

- [8] T. Prosen, *Phys. Rev. Lett.* **112**, 030603 (2014).
- [9] P. Ribeiro, A. E. Antipov, and A. N. Rubtsov, *Phys. Rev. B* **93**, 144305 (2016).
- [10] J. Lang and F. Piazza, [arXiv:1602.05102](https://arxiv.org/abs/1602.05102).
- [11] L. M. Sieberer, M. Buchhold, and S. Diehl, [arXiv:1512.00637](https://arxiv.org/abs/1512.00637).
- [12] J. Marino and S. Diehl, *Phys. Rev. Lett.* **116**, 070407 (2016).
- [13] R. A. Barankov, L. S. Levitov, and B. Z. Spivak, *Phys. Rev. Lett.* **93**, 160401 (2004).
- [14] E. A. Yuzbashyan, O. Tsyplatyev, and B. L. Altshuler, *Phys. Rev. Lett.* **96**, 097005 (2006).
- [15] E. A. Yuzbashyan and M. Dzero, *Phys. Rev. Lett.* **96**, 230404 (2006).
- [16] R. A. Barankov and L. S. Levitov, *Phys. Rev. Lett.* **96**, 230403 (2006).
- [17] M. Eckstein, M. Kollar, and P. Werner, *Phys. Rev. Lett.* **103**, 056403 (2009).
- [18] M. Schiró and M. Fabrizio, *Phys. Rev. Lett.* **105**, 076401 (2010).
- [19] B. Sciolla and G. Biroli, *Phys. Rev. Lett.* **105**, 220401 (2010).
- [20] M. Schiró and M. Fabrizio, *Phys. Rev. B* **83**, 165105 (2011).
- [21] N. Tsuji, M. Eckstein, and P. Werner, *Phys. Rev. Lett.* **110**, 136404 (2013).
- [22] B. Sciolla and G. Biroli, *Phys. Rev. B* **88**, 201110 (2013).
- [23] H.-J. Lee and R. Bulla, *Eur. Phys. J. B* **56**, 199 (2007).
- [24] H.-J. Lee, K. Byczuk, and R. Bulla, *Phys. Rev. B* **82**, 054516 (2010).
- [25] J. Warnes and E. Miranda, *Eur. Phys. J. B* **85**, 341 (2012).
- [26] J. Kondo, *Prog. Theor. Phys.* **32**, 37 (1964).
- [27] Q. Si, S. Rabello, K. Ingersent, and J. L. Smith, *Nature (London)* **413**, 804 (2001).
- [28] M. Vojta, *Philos. Mag.* **86**, 1807 (2006).
- [29] A. Bayat, H. Johannesson, S. Bose, and P. Sodano, *Nat. Commun.* **5**, 3784 (2014).
- [30] K. Ingersent and Q. Si, *Phys. Rev. Lett.* **89**, 076403 (2002).
- [31] K. L. Hur, *Understanding Quantum Phase Transitions* (CRC Press, Boca Raton, FL, 2010), p. 217.
- [32] F. Heidrich-Meisner, A. E. Feiguin, and E. Dagotto, *Phys. Rev. B* **79**, 235336 (2009).
- [33] P. Werner, T. Oka, M. Eckstein, and A. J. Millis, *Phys. Rev. B* **81**, 035108 (2010).
- [34] A. E. Antipov, Q. Dong, and E. Gull, *Phys. Rev. Lett.* **116**, 036801 (2016).
- [35] Y. E. Shchadilova, P. Ribeiro, and M. Haque, *Phys. Rev. Lett.* **112**, 070601 (2014).
- [36] S. Ghosh, P. Ribeiro, and M. Haque, *J. Stat. Mech.: Theory Exp.* (2015) P08002.
- [37] A. Shashi, F. Grusdt, D. A. Abanin, and E. Demler, *Phys. Rev. A* **89**, 053617 (2014).
- [38] M. Knap, A. Shashi, Y. Nishida, A. Imambekov, D. A. Abanin, and E. Demler, *Phys. Rev. X* **2**, 041020 (2012).
- [39] R. Schmidt, H. R. Sadeghpour, and E. Demler, *Phys. Rev. Lett.* **116**, 105302 (2016).
- [40] M. Schiró, *Phys. Rev. B* **86**, 161101 (2012).
- [41] M. Schiró, *Phys. Rev. B* **81**, 085126 (2010).
- [42] P. P. Orth, A. Imambekov, and K. Le Hur, *Phys. Rev. B* **87**, 014305 (2013).
- [43] L. Henriot, Z. Ristivojevic, P. P. Orth, and K. Le Hur, *Phys. Rev. A* **90**, 023820 (2014).
- [44] T. Cizmar, M. Mazilu, and K. Dholakia, *Nat. Photonics* **4**, 388 (2010).
- [45] J. K. Freericks and H. Monien, *Europhys. Lett.* **26**, 545 (1994).
- [46] P. Anders, E. Gull, L. Pollet, M. Troyer, and P. Werner, *Phys. Rev. Lett.* **105**, 096402 (2010).
- [47] G. Roux, *Phys. Rev. A* **79**, 021608 (2009).
- [48] G. Roux, *Phys. Rev. A* **81**, 053604 (2010).
- [49] J. M. Zhang, C. Shen, and W. M. Liu, *Phys. Rev. A* **83**, 063622 (2011).
- [50] M. Snoek, *Europhys. Lett.* **95**, 30006 (2011).
- [51] C. Trefzger and K. Sengupta, *Phys. Rev. Lett.* **106**, 095702 (2011).
- [52] S. Sorg, L. Vidmar, L. Pollet, and F. Heidrich-Meisner, *Phys. Rev. A* **90**, 033606 (2014).
- [53] B. Kain and H. Y. Ling, *Phys. Rev. A* **90**, 063626 (2014).
- [54] H. U. R. Strand, M. Eckstein, and P. Werner, *Phys. Rev. X* **5**, 011038 (2015).
- [55] F. A. Wolf, I. P. McCulloch, O. Parcollet, and U. Schollwöck, *Phys. Rev. B* **90**, 115124 (2014).
- [56] K. Balzer and M. Eckstein, *Phys. Rev. B* **89**, 035148 (2014).
- [57] N. E. Bickers, *Rev. Mod. Phys.* **59**, 845 (1987).
- [58] A. V. Andreev, V. I. Emel'yanov, and Y. A. Il'inskiĭ, *Sov. Phys. Usp.* **23**, 493 (1980).
- [59] R. H. Dicke, *Phys. Rev.* **93**, 99 (1954).